Research Article | Vol. 25, No. 10 | 15 May 2017 | OPTICS EXPRESS 11637

Optics EXPRESS

Reflection of few cycle laser pulses from an inhomogeneous overdense plasma

S. K. MISHRA,[1,*] A. ANDREEV,[1,2] AND M. P. KALASHINIKOV[1,2]

[1]*ELI-Attosecond Light Pulse Source, Szeged, Hungary*
[2]*Max Born Institute (MBI), Berlin, Germany*
**mishra.sk@eli-alps.hu*

Abstract: The use of a plasma mirror to improve the temporal contrast of few cycle laser pulses has been considered. Pre-plasma features, prior to the main pulse, have been evaluated using an analytical model that has been verified using hydrodynamic code. The temporal/ spectral profile, reflectivity, and broadening of the reflected pulse have been parametrically analysed using an analytical formulation that describes the reflection of broadband ultra-short pulses from the plasma gradient. The analytical estimate for the pulse reflectivity is in good agreement with experimental measurements. The consistency of the analytical expressions for the collisionless case has been validated via comparison with a 1D particle in cell simulations.

OCIS codes: (140.0140) Lasers and laser optics; (350.5400) Plasmas; (120.5700) Reflection.

References and links

1. D. Strickland and G. Mourou, "Compression of amplified chirped optical pulses," Opt. Commun. **56**(3), 219–221 (1985).
2. M. Kalashnikov, A. Andreev, and H. Schönnagel, "Limits of the temporal contrast for CPA lasers with beams of high aperture," Proc. SPIE **7501**, 750104 (2009).
3. N. V. Didenko, A. V. Konyashchenko, A. P. Lutsenko, and S. Y. Tenyakov, "Contrast degradation in a chirped-pulse amplifier due to generation of prepulses by postpulses," Opt. Express **16**(5), 3178–3190 (2008).
4. N. Khodakovskiy, M. Kalashnikov, E. Gontier, F. Falcoz, and P.-M. Paul, "Degradation of picosecond temporal contrast of Ti:sapphire lasers with coherent pedestals," Opt. Lett. **41**(19), 4441–4444 (2016).
5. I. Watts, M. Zepf, E. L. Clark, M. Tatarakis, K. Krushelnick, A. E. Dangor, R. Allott, R. J. Clarke, D. Neely, and P. A. Norreys, "Measurements of relativistic self-phase-modulation in plasma," Phys. Rev. E Stat. Nonlin. Soft Matter Phys. **66**(3), 036409 (2002).
6. D. Umstadter, "Review of physics and applications of relativistic plasmas driven by ultra-intense lasers," Phys. Plasmas **8**(5), 1774–1785 (2001).
7. M. D. Perry and G. Mourou, "Terawatt to petawatt subpicosecond lasers," Science **264**(5161), 917–924 (1994).
8. F. Brunel, "Not-so-resonant, resonant absorption," Phys. Rev. Lett. **59**(1), 52–55 (1987).
9. M. Grimes, A. Rundquist, Y. Lee, and M. Downer, "Experimental identification of vacuum heating at femtosecond-laser-irradiated metal surfaces," Phys. Rev. Lett. **82**(20), 4010–4013 (1999).
10. M. P. Kalashnikov, E. Risse, H. Schönnagel, and W. Sandner, "Double chirped-pulse-amplification laser: a way to clean pulses temporally," Opt. Lett. **30**(8), 923–925 (2005).
11. A. Jullien, O. Albert, F. Burgy, G. Hamoniaux, J.-P. Rousseau, J.-P. Chambaret, F. Augé-Rochereau, G. Chériaux, J. Etchepare, N. Minkovski, and S. M. Saltiel, "10^{-10} temporal contrast for femtosecond ultraintense lasers by cross-polarized wave generation," Opt. Lett. **30**(8), 920–922 (2005).
12. V. Chvykov, P. Rousseau, S. Reed, G. Kalinchenko, and V. Yanovsky, "Generation of 10^{11} contrast 50 TW laser pulses," Opt. Lett. **31**(10), 1456–1458 (2006).
13. M. P. Kalashnikov, H. Schönnagel, and W. Sandner, "High temporal contrast front end with a CaF_2CaF_2-based XPW temporal filter for high intensity lasers," AIP Conf. Proc. **1465**, 13–17 (2012).
14. H. Liebetrau, M. Hornung, A. Seidel, M. Hellwing, A. Kessler, S. Keppler, F. Schorcht, J. Hein, and M. C. Kaluza, "Ultra-high contrast frontend for high peak power fs-lasers at 1030 nm," Opt. Express **22**(20), 24776–24786 (2014).
15. M. P. Kalashnikov, K. Osvay, G. Priebe, L. Ehentraut, S. Steinke, and W. Sandner, "Temporal contrast of high intensity laser systems above 10^{11} with double CPA technique," AIP Conf. Proc. **1462**, 108–111 (2012).
16. H. C. Kapteyn, M. M. Murnane, A. Szoke, and R. W. Falcone, "Prepulse energy suppression for high-energy ultrashort pulses using self-induced plasma shuttering," Opt. Lett. **16**(7), 490–492 (1991).
17. D. M. Gold, H. Nathel, P. R. Bolton, W. E. White, and L. D. V. Woerkom, "Short pulse high intensity lasers and applications," Proc. SPIE **1413**, 41–52 (1991).
18. S. Backus, H. C. Kapteyn, M. M. Murnane, D. M. Gold, H. Nathel, and W. White, "Prepulse suppression for high-energy ultrashort pulses using self-induced plasma shuttering from a fluid target," Opt. Lett. **18**(2), 134–136 (1993).

#284558 https://doi.org/10.1364/OE.25.011637
Journal © 2017 Received 13 Jan 2017; revised 16 Mar 2017; accepted 17 Mar 2017; published 20 Apr 2017

Optics EXPRESS

19. D. M. Gold, "Direct measurement of prepulse suppression by use of a plasma shutter," Opt. Lett. **19**(23), 2006–2008 (1994).
20. Z. Bor, B. Racz, G. Szabo, D. Xenakis, C. Kalpouzos, and C. Fotakis, "Femtosecond transient reflection from polymer surfaces during femtosecond UV photoablation," Appl. Phys., A Mater. Sci. Process. **60**(4), 365–368 (1995).
21. Ch. Ziener, P. S. Foster, E. J. Divall, C. J. Hooker, M. H. R. Hutchinson, A. J. Langley, and D. Neely, "Specular reflectivity of plasma mirrors as a function of intensity, pulse duration, and angle of incidence," J. Appl. Phys. **93**(1), 768–770 (2003).
22. P. Monot, G. Doumy, S. Dobosz, M. Perdrix, P. D'Oliveira, F. Quéré, F. Réau, P. Martin, P. Audebert, J.-C. Gauthier, and J.-P. Geindre, "High-order harmonic generation by nonlinear reflection of an intense high-contrast laser pulse on a plasma," Opt. Lett. **29**(8), 893–895 (2004).
23. G. Doumy, F. Quéré, O. Gobert, M. Perdrix, P. Martin, P. Audebert, J.-C. Gauthier, J.-P. Geindre, and T. Wittmann, "Complete characterization of a plasma mirror for the production of high-contrast ultraintense laser pulses," Phys. Rev. E Stat. Nonlin. Soft Matter Phys. **69**(2), 026402 (2004).
24. C. Thaury, F. Quéré, J.-P. Geindre, A. Levy, T. Ceccotti, P. Monot, M. Bougeard, F. Réau, P. d'Oliveira, P. Audebert, R. Marjoribanks, and Ph. Martin, "Plasma mirrors for ultrahigh-intensity optics," Nat. Phys. **03**(6), 424–429 (2007).
25. T. Wittmann, *Thesis: Complete Characterization of Plasma Mirrors and Development of a Single Shot Carrier-Envelope Phase Meter* (University of Szeged, 2009).
26. G. G. Scott, V. Bagnoud, C. Brabetz, R. J. Clarke, J. S. Green, R. I. Heathcote, H. W. Powell, B. Zielbauer, T. D. Arber, P. McKenna, and D. Neely, "Optimization of plasma mirror reflectivity and optical quality using double laser pulses," New J. Phys. **17**(3), 033027 (2015).
27. A. Borot, D. Douillet, G. Iaquaniello, T. Lefrou, P. Audebert, J.-P. Geindre, and R. Lopez-Martens, "High repetition rate plasma mirror device for attosecond science," Rev. Sci. Instrum. **85**(1), 013104 (2014).
28. B. H. Shaw, S. Steinke, J. van Tilborg, and W. P. Leemans, "Reflectance characterization of tape-based plasma mirrors," Phys. Plasmas **23**(6), 063118 (2016).
29. C. Rödel, M. Heyer, M. Behmke, M. Kübel, O. Jäckel, W. Ziegler, D. Ehrt, M. C. Kaluza, and G. G. Paulus, "High repetition rate plasma mirror for temporal contrast enhancement of terawatt femtosecond laser pulses by three orders of magnitude," Appl. Phys. B **103**(2), 295–302 (2011).
30. ELI-ALPS web page for primary laser parameters: http://www.eli-hu.hu/
31. G. A. Mourou, G. Korn, W. Sandner, and J. L. Collier, eds., *ELI White Book: Science and Technology with Ultra-Intense Lasers* (Andreas Thos, 2011).
32. A. Sotnikov, H. Laux, and B. Stritzker, "Experimental and numerical optimization of beam shapes for short-pulse ultraviolet laser cutting processing," Phys. Procedia **05**(6), 137–146 (2010).
33. R. Lichters, R. E. W. Pfund, and J. Meyer-ter-Vehn, *LPIC + +, Report No. MPQ* 225 (Max-Planck Institute of Quantum Optics, 1997).
34. S. Kozaki and Y. Mushiake, "Propagation of the electromagnetic pulse with Gaussian envelope in inhomogeneous ionized media," IEEE Trans. Antenn. Propag. **17**(5), 686–688 (1969).
35. K. P. Singh, P. K. Shukla, and R. N. Singh, "Propagation of an electromagnetic pulse through inhomogeneous plasmas," Int. J. Electron. **30**(03), 249–254 (1971).
36. Y. Shiau and R. F. H. Yang, "Distortion of a radio pulse reflected from an inhomogeneous lossy plasma," Proc. IEEE **60**(1), 142–143 (1972).
37. M. D. Perry, T. Ditmire, and B. C. Stuart, "Self-phase modulation in chirped-pulse amplification," Opt. Lett. **19**(24), 2149–2151 (1994).
38. B. Kohler, V. V. Yakovlev, K. R. Wilson, J. Squier, K. W. Delong, and R. Trebino, "Phase and intensity characterization of femtosecond pulses from a chirped-pulse amplifier by frequency-resolved optical gating," Opt. Lett. **20**(5), 483–485 (1995).
39. K. G. Budden, *Radio Waves in the Ionosphere* (Cambridge University, 1961), Chap.8 & Chap.16.
40. T. Zh. Esirkepov, J. K. Koga, A. Sunahara, T. Morita, M. Nishikino, K. Kageyama, H. Nagatomo, K. Nishihara, A. Sagisaka, H. Kotaki, T. Nakamura, Y. Fukuda, H. Okada, A. S. Pirozhkov, A. Yogo, M. Nishiuchi, H. Kiriyama, K. Kondo, M. Kando, and S. V. Bulanov, "Prepulse and amplified spontaneous emission effects on the interaction of a PW class laser with thin solid targets," Nucl. Instrum. Methods Phys. Res. A **745**(05), 150–163 (2014).
41. A. Djaui, "A user guide for the laser plasma simulation code: Med-103," Technical Report: RAL-TR-96–099 (1996).
42. V. A. Isakov, A. P. Kanavin, and S. A. Uryupin, "Reflection and absorption of a high-power ultra-short laser pulse heating a solid-state target," Laser Part. Beams **23**(03), 315–319 (2005).
43. J. D. Huba, *NRL Plasma Formulary* (Office of Naval Research, 2013).
44. P. L. Poole, A. Krygier, G. E. Cochran, P. S. Foster, G. G. Scott, L. A. Wilson, J. Bailey, N. Bourgeois, C. Hernandez-Gomez, D. Neely, P. P. Rajeev, R. R. Freeman, and D. W. Schumacher, "Experiment and simulation of novel liquid crystal plasma mirrors for high contrast, intense laser pulses," Sci. Rep. **6**(1), 32041 (2016).

Optics EXPRESS

1. Introduction

Current high intensity laser experiments principally use chirped pulse amplification (CPA) techniques [1] in producing ultrashort (sub ps) high intensity electromagnetic (EM) pulses. The emerging pulses have nanosecond (ns) and picosecond (ps) temporal peculiarities before the main pulse. These features are attributed to amplified spontaneous emission (ASE), spectral phase mismatch, pre-pulses generated from post-processing and scattering from the optical elements, etc [2–4], that appear in CPA operation. Such temporal peculiarities are characterized by the intensity contrast (K), which is defined as the ratio of peak intensity of the pulse to the instant intensity i.e. $K = (I_{max}/I)$. The temporal contrast is of immense significance to the modern relativistic laser plasma experiments. Temporal fluctuations, in the form of pre-pulses that exceed ionization threshold [2], trigger a detrimental inhomogeneous pre-plasma on the irradiated side of the target; in addition this also alters the target features. The subsequent inhomogeneous pre-plasma inhibits the interaction of the main pulse with steep density target and significantly alters the outcome. The pulse with weaker contrast encumbers rigorous diagnostics of the laser-matter interaction phenomena [5–9] and thus high contrast pulses are required in order to perform efficient experimental campaigns.

High temporal contrast in CPA systems is currently achieved by using the Double-CPA (DCPA) technique [10] – a combination with temporal filtering based on generation of cross-polarized wave (XPW) [11]. This technique has been successfully demonstrated to operate with Ti: Sapphire [12, 13] and Yb–doped lasers [14]. ASE levels in the next generation of laser systems can be successfully reduced using DCPA, however the maximum ASE temporal contrast is limited by the damage threshold of diffraction gratings in the stretcher to the value of ~10^{15} [15]. Recompressed pulses contain several other features, in addition to ASE, during amplification. These include coherent pre-pulses [3] and pedestals [4] generated from post-radiation in the second CPA stage. XPW cannot be applied in to high energy recompressed pulses used in multi-Terawatt (TW) and Petawatt (PW) laser systems. Thus other methods of temporal filtering, particularly the self-induced plasma mirror [16–26] has emerged as a preferred scheme for pedestal/pre-pulse suppression and generation of high contrast ultra-short pulses with a steep leading front.

The conceptual basis of self-induced plasma mirrors (PMs) is quite simple. Laser light is focused on a low reflectivity target surface and some of the pre-pulse energy is transmitted through the target. As the pre-pulse passes through, the target gets ionized depending on the temporal intensity of pre-pulse or leading edge; the hydrodynamic expansion further leads the formation of inhomogeneous plasma [25]. Increased level of ionization may result in the plasma density exceeding the critical value and at this stage the target surface becomes a plasma mirror. This results in significant reflection of incident main pulse with improved contrast. The fluence of pre-pulse is crucial in configuring PMs and should be optimized in achieving significant contrast [23]. Recent studies are focusing on the optimization of PMs with different setups and gauging its feasibility to large scale experiments [16–25]. In [23], the PM is formed under combined influence of leading edge of main pulse (I_{max} ~10^{15} Wcm^{-2}, ~60 fs) and the pedestal. The measured contrast is approximately six orders of magnitude on the ns time scale before the main pulse. In their work, the importance of threshold fluence for the reflectivity from quartz is highlighted; further they report ~60% reflectivity for ~60 J cm^{-2} pulse. Another concern with PMs is that every shot damages the target and subsequent shots require quick positioning of fresh target plates during experiment. This becomes significant when using laser pulses with a high repetition rate. In this context, numerous techniques to achieve active solid target positioning for driving plasma mirrors at high repetition rate (~KHz) has been proposed in recent investigations [27,28]. In addition, PMs configured with high repetition also improve the temporal contrast of the pulse. For example, a PM operating [29] with ~10 Hz repetition rate at JETI configuration, an intense pulse (~TW fs) results in an enhanced contrast of ~10^{5}-10^{8} (at ~ps time scale) and ~80% peak reflectivity. Considering the

Optics EXPRESS

parameters of primary lasers [30,31] foreseen to operate at ELI-ALPS, PM could be a promising setup in achieving clean high intensity ultra-short pulses.

Laser pulses at ELI-ALPS facility [30] will have few cycle durations. Plasma mirrors will be required as pre-pulses, ASE and additional features at the leading edge are unavoidable in any laser system. Plasma mirror is typically followed by other optical elements as turning mirrors, focusing optics, etc. These can introduce an additional impact on the spectral phase lengthening of the pulse as well as the spectral phase. Plasma mirrors may compensate for these effects when used in conjunction with a spectrally stretched pulse [32]. This requires a detailed investigation of the plasma mirror applied for very broad band pulses. In this investigation, we have analytically examined the reflection of ultrashort (broad spectrum) laser pulses from PM created by pre-pulse/ pedestal associated with the main pulse. The PM is defined as an inhomogeneous plasma with high (solid) density gradient. The Fourier correlation $\Delta\omega\cdot\Delta\tau \geq 2\pi f$ specifies the spectral broadening associated with finite duration pulse where Δ refers the FWHM associated with temporal and spectral profile of the pulse while f is a shape dependent constant (for Gaussian shape f~0.44). Ultrashort pulses have a broad spectrum and each frequency component reflects from different plasma layer adjacent to the critical plasma density. The analysis is simplified by an initial calculation of the PM through the pre-pulse target interaction by material ionization (plasma generation) and hydrodynamics expansion. The reflection of the main short pulse is then modeled using this preformed plasma region (PM). The pre-plasma features have been evaluated by an analytical model, followed by laser plasma simulation hydrodynamic code. The output of the hydrodynamic code (the pre-plasma profile) has been coupled with analytical formulation for the pulse reflection in order to evaluate the characteristic features of reflected pulse. The analytical expressions for the pulse reflectivity have been validated with experimental observations and are further used for the parametric analysis of the short pulse after reflection from the sharp boundaries of self-induced PMs. The temporal/spectral profile, peak reflectivity and broadening have been evaluated as a function of plasma inhomogeneity. Particle in cell (PIC) simulation, using 1D code LPIC [33], has been performed to verify the analytical predictions.

The manuscript begins with a linear analysis characterizing short pulse reflection from the pre-plasma in Section 2. The pre-plasma formation due to hydrodynamic expansion has been described in Section 3. The numerical results for the reflection of short pulses from PM based on analytical expressions have been discussed in Section 4. This is followed by 1D PIC simulation results in Section 5 and a summary of the outcome of this study (in Section 6) concludes the paper.

2. Evaluation of pulse profile after reflection

In this section, we evaluate the profile of ultrashort intense pulses after reflection from the preformed inhomogeneous plasma. Considering the intense pre-pulse interaction for a short (~ps) time scale, the plasma inhomogeneity over target surface can be simply specified by a linear ramp profile – the plasma density may span from a minimum up to several times the critical density. For simplicity, the algebraic form of the plasma inhomogeneity (along z–axis) is taken as $n_e = bz$, where b is the density steepness (inhomogeneity parameter). The pulse is considered to incident on inhomogeneous plasma slab interface (xy plane) at $z = 0$ and the density linearly increases with $z > 0$. A sketch of the coordinate scaling has been shown in Fig. 1. A linearly polarized EM pulse (with s-polarization and yz plane – plane of incidence) propagating in direction, making an angle θ with z-axis, can be written as [34–36]

$$E_i(y,z,t) = \int_{-\infty}^{\infty} E_i(\omega) exp\left[i\{\omega t - k(y\sin\theta + z\cos\theta)\}\right] d\omega, \quad (1)$$

Optics EXPRESS

where $k(=\omega/c)$ is wave number, $E_i(\omega)$ refers frequency spectrum associated with incident pulse $E_i(t)$ and can be expressed as $E_i(\omega)=\int_{-\infty}^{\infty}E_i(t)exp(-i\omega t)dt$.

It should be stated that the present analysis takes into account a linear density profile of the plasma (instead of an exponential profile), in order to achieve a simple analytical solution; such specific expressions are difficult to achieve in the case of exponential decay. The linear profile considered herein, is justified as the reflection of the pulse occurs in the region close to the critical plasma density. This specific region in the exponential decay can be approximated as a linear ramp with adequate steepness (b). It is helpful to have a notion of the scale length correlation between the linear and exponential decay profiles. In case of the linear ramp profile, the plasma density terminates at $z_p=n_o/b$, where n_o refers the plasma density on the target surface (corresponding to the maximum ionization). Similarly, for the exponential decay, the plasma may extend up to few (say q) times density scale length (l_e) *i.e.* ~ql_e where l_e is the extension length from the target surface where the plasma density drops to a fraction of ($1/e$). The scale lengths in the two aforementioned cases may crudely be correlated as $z_p=n_o/b=ql_e\Rightarrow l_e/b=(n_o/q)$. Herein for the analysis, the sinusoidal carrier with a Gaussian pulse envelope is defined as

$$E_i(t)=E_o exp(-t^2/2\tau^2)exp[i(\omega_o t+\phi_0)], \tag{2}$$

where ω_o, τ and E_o respectively refer central frequency, width and electric field amplitude of the pulse while δ corresponds to the chirp phase associated with incident pulse. This chirp phase evolves in the pulse generation process during compression/stretching techniques and usually has complex dependence on the pulse spectrum [37,38]. In order to avoid the complexity in algebraic analysis $\phi_0=0$ has been set for further analysis: this refers to the transform-limited case where the chirp components i.e., compressor, stretcher and material, are retained so that there is net zero dispersion. Alongwith this simplification, Gaussian pulse (Eq. (2) corresponds to Gaussian spectra in $\omega-$ space as

$$E_i(\omega)=E_o(2\pi)^{1/2}\tau exp[-(\tau^2/2)(\omega-\omega_o)^2]. \tag{3}$$

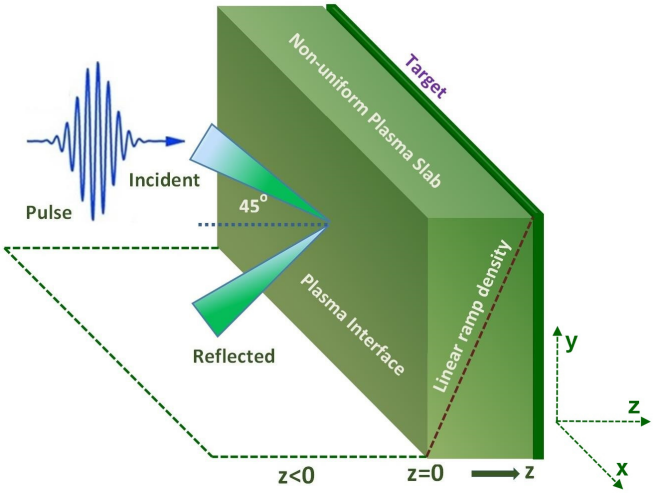

Fig. 1. A schematic of pulse reflection and coordinate scaling from ramp profile preformed plasma (PM).

In this framework, a finite duration pulse is considered as manifestation of various frequency components via its spectral distribution and each frequency component is reflected

Optics EXPRESS

from different density layer as it advances through the inhomogeneous plasma. Following earlier analysis [34,35,39], the coefficient of reflection, corresponding to a linear ramp density profile (with finite collisions), can approximately be expressed as

$$r = exp[-(i+\eta)\varphi_\omega + i\pi/2], \tag{4}$$

where $\varphi_\omega = 2\kappa\omega^3$, $\kappa = (2/3)cos^3\theta/\alpha_o c$, $\alpha_o = e^2 b/m_e\varepsilon_0$, $\eta = \nu/\omega$ and ν is the collision frequency. For the reflection coefficient r, the amplitude of the reflected pulse corresponding to a particular frequency component is modulated as $E_r(\omega) = rE_i(\omega)$ and its waveform can be written as $E_r = rE_i(\omega)exp(i\omega t')$, where $t' = t - (k/\omega)(ysin\theta - zcos\theta)$. The temporal profile of the reflected pulse may be obtained by performing an inverse Fourier transformation of the reflected spectra and can be expressed as

$$\begin{aligned} E_r(y,z,t) &= (1/2\pi)\int_{-\infty}^{\infty} rE_i(\omega)exp(i\omega t')\ d\omega \\ &= (2\pi)^{-1/2} e^{i\pi/2} E_o \tau\left[\int_{-\infty}^{\infty} exp[-(i+\eta)\varphi_\omega - (\tau^2/2)(\omega-\omega_o)^2 + i\omega t']\ d\omega\right] \end{aligned} \tag{5}$$

Equation (5) describes the envelope/ phase information of pulse after reflection. For a narrow band spectrum of the pulse i.e. $\delta\omega/\omega_o \sim (\omega-\omega_o)/\omega_o << 1$, the integration is dominated by the central frequency ω_o. In order to obtain an analytical solution, this integral (Eq. (5) can further be simplified using Tailor's expansion for the parameter φ_ω around the central frequency ω_o as $\varphi_\omega = \sum_{j=0}^{j}(\omega-\omega_o)^j(\partial_\omega\varphi_\omega/j!)_{\omega_o}$.

Coupling this expansion of φ_ω with Eq. (5) and retaining the terms up to third term, the solution of the reflected pulse can be expressed as

$$E_r(y,z,t) = E_{ro}exp(i\Delta)exp(i\omega_o t'), \tag{6}$$

where

$$E_{ro} = \frac{E_o exp(-\eta\varphi_{\omega_o})}{[\chi^2 + (1+\chi\eta)^2]^{1/4}} exp\left(-\frac{[(\varphi'_{\omega_o} - t')^2 - \varphi'^2_{\omega_o}\eta^2](1+\chi\eta) - 2\chi\eta(\varphi'_{\omega_o} - t')\varphi'_{\omega_o}}{2\tau^2[\chi^2 + (1+\chi\eta)^2]}\right) \tag{7}$$

and

$$\Delta \equiv \left(\frac{\pi}{2} - \varphi_{\omega_o} - \frac{1}{2}tan^{-1}\frac{\chi}{(1+\chi\eta)} + \frac{[(\varphi'_{\omega_o} - t')^2 - \varphi'^2_{\omega_o}\eta^2]\chi + 2\varphi'_{\omega_o}\eta(\varphi'_{\omega_o} - t')(1+\chi\eta)}{2\tau^2[\chi^2 + (1+\chi\eta)^2]}\right) \tag{8}$$

refers the temporal envelop of the reflected pulse and phase with $\chi = \varphi''_{\omega_o}/\tau^2$, $\varphi_{\omega_o} = 2\kappa\omega_o^3$, $\varphi'_{\omega_o} = 6\kappa\omega_o^2$, $\varphi''_{\omega_o} = 12\kappa\omega_o$ and $\varphi'''_{\omega_o} = 12\kappa$.

The expression (Eq. (7) describes the distortion of the pulse envelop after reflection even in the collisionless case ($\eta = 0$) and displays the subsequent delay by a group time $\tau_g \approx \varphi'_{\omega_o} \sim 4\omega_o^2 cos^3\theta/\alpha_o c$. Further, χ is crucial parameter which controls the pulse distortion. When $\chi << 1$, the pulse maintains a Gaussian profile ($E_{ro} \sim exp[-(\varphi'_{\omega_o} - t')^2/2\tau^2]$) after its reflection while in the case when the parameter $\chi >> 1$, the reflected pulse envelop deforms as $\sim \chi^{-1/2} exp[-(\varphi'_{\omega_o} - t')^2/2\tau^2\chi^2]$. Consistently with Eq. (7), envelop broadening is anticipated in the case of short wavelength (λ_o), small angle of incidence (θ) and weak inhomogeneity (b). This may be physically attributed to a larger penetration in inhomogeneous plasma with

Optics EXPRESS

broader frequency spectrum and large phase difference between incident and reflected pulse. The collisions (finite η) effectively reduce the amplitude and the phase of the reflected pulse. In this analysis, the collision term has been used to understand the effects of damping, which might include all possible collisional/ resistive effects whether it originates from the particle collisions or via classical absorption. Refined mechanisms like skin effect/ individual collisions have not been included explicitly in this analysis. It should also be mentioned that the present formulation is based on the constant steepness b while in the realistic scenario of PMs the plasma expansion may coexist with main pulse interaction. In this case, it may reduce the plasma steepness during interaction i.e., lower b. Nonetheless, this constant steepness formulation can be safely applied if the main pulse is short enough in comparison to the pre-pulse, as in this scenario. The frequency spectrum of the reflected pulse is obtained using Fourier transform of pulse envelop (Eq. (6) and can be algebraically expressed as

$$E_r(\omega) = \int_{-\infty}^{\infty} E_r(t) exp(j\omega t) dt. \tag{9}$$

It should be emphasized that few simplifications were made in obtaining analytical solutions but the outcome gives the physical notion about the short pulse reflection from a dense inhomogeneous plasma medium.

3. Evaluation of plasma inhomogeneity

3.1 Simple model for pre-plasma formation

An electromagnetic (EM) pulse is characterized by peak intensity with a finite spectral bandwidth and temporally may extend up to a few laser cycles. This may include pre-pulse/ pedestal exceeding threshold fluence. When the radiation (EM pulse) encounters a solid target, the pre-pulse/ pedestal causes ionization of surface material and plasma heating due to Ohmic/ collisional effects. The heating induces an expansion of the surface plasma. The two effects describing the density and plasma temperature on the surface [40] can be written as

$$\partial n_e / \partial t = f_i (n_o - n_e) \tag{10}$$

$$\partial T_e / \partial t = \left(\frac{e^2 \left| E_p \right|^2}{m_e (\nu^2 + \omega_o^2)} - \delta_{ei} (T_e - T_o) \right) \nu \tag{11}$$

where, $f_i = [\sigma_l (I_p / \hbar\omega_o)^l + \beta (n_e / n_o) I_p]$ is the rate of electron excitation from valance to conduction band in solid. These two terms in the parenthesis of f_i refer to the multi-photon ionization and electronic avalanche respectively, n_o corresponds to the bound electron density in target, E_p (I_p) refers field (intensity) of the pedestal, l is the minimum number of photons required to overcome the band gap, σ_l is collision cross-section, $\nu = \nu_o (n_e / n_{e0})(T_e / T_{e0})^{-3/2}$, $\nu_o = 4.4 \times 10^{12}$ s^{-1} (for $n_{e0} = 10^{21}$ cm^{-3} and $T_{e0} = 100$ eV) and T_o is surrounding temperature. For quartz (silica) [23]: $\delta_{oi} = (2m_e / m_i) \sim 2 \times 10^{-5}$, $\sigma_l = 2.3 \times 10^{-178}$ cm^{12}s^{-5}, $\beta = 11$ cm^{2}J^{-1}, $l = 6$ (corresponding to the band gap ~10 V and ~800 nm laser) and $n_o = 4.25 \times 10^{23}$ cm^{-3}. For all practical purposes finite duration (FWHM~τ_p) pre-pulse/ pedestal can be chosen of Gaussian shape as $I_p = I_{po} exp[-4ln2(t^2 / \tau_p^2)]$.

The plasma generation and subsequent expansion primarily depends on incident energy (or fluence) and interaction time. For the present analysis, contrast ratio similar to recent studies [23, 29] are chosen which for the TW laser is reasonably corresponds to a pre-pulse intensity of the order of $I_{po} \sim 10^{12}$ Wcm^{-2}; this may be above threshold fluence. Next, Eqs. (10-11) have been solved numerically for quartz (silica) parameters and corresponding n_e and T_e on the target surface is obtained. In calculations, the electron density at surface is found to

Optics EXPRESS

sharply approach towards maximum value n_o for the fluence $\in$ (1-5) Jcm^{-2}, with I_{po}~10^{12} Wcm^{-2}, τ_p~1-5 ps while the electron temperature is seen to be an increasing function of the pre-pulse intensity. The speed of plasma expansion may be approximated as ion sound speed at the end of pre-pulse and can be expressed as $\upsilon_s = 9.79\times10^5 (ZT_e / m_i)^{1/2}$ cms^{-1}. This is a reasonable approximation for ~ps pre-pulses, while in case of shorter pre-pulses $\leq 1ps$ the electron thermal motion is more significant [23] in describing the pre-plasma expansion. Assuming the interaction time is equal to the pedestal/pre-pulse duration, the plasma extension length can be written as $L \approx \upsilon_s \tau_p$. Considering linear ramp density profile in pre-formed plasma, the inhomogeneity parameter can be estimated as the ratio of peak density at the surface to the expansion length i.e., $b \approx n_o / L$. The analytical estimate for inhomogeneity parameter (b) has been illustrated as a function of pre-pulse/ pedestal FWHM (τ_p) by blue curve in Fig. 2. The inhomogeneity parameter's magnitude is of the order of $\sim 10^{27}$ cm^{-4}.

3.2 Plasma expansion using hydrodynamic code MEDUSA

A further quantitative scaling of the pre-plasma formation, expansion and its profile due to the pre-pulse/ pedestal interacting with solid target has been conducted using the Laser plasma simulation hydro code MEDUSA (MED-103) [41]. In the simulation, the pre-pulse can be described as a Gaussian pulse with a peak intensity according to the contrast ratio of main pulse. The pre-pulse interacts with a quartz (silica, SiO_2, mass 60 amu) surface target with planar geometry. This pre-pulse may lead the surface to maximum ionization and plasma density equivalent to $n_o = 4.25\times10^{23}$ cm^{-3} (corresponding to O^{6+} and Si^{4+} ionization state).

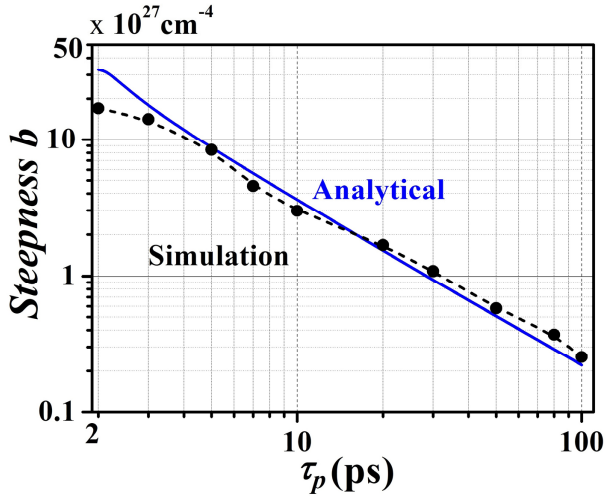

Fig. 2. Steepness (b) as function τ_p for I_{po}~10^{12} Wcm^{-2}. The blue and black curves (with dots) correspond to analytical and hydrodynamic code estimates respectively.

After the simulation run, the inhomogeneous plasma expansion over the surface is seen to have a trapezium shape with a peak density n_o and extended up to sub-micron scale length. In the context of present analysis, taking hydrodynamic plasma expansion into account, the steepness (b) has been evaluated as gradient of the sharp falling part of the trapezium profile, obtained in simulation. Utilizing the numerous set of simulation runs, the steepness parameter b has been evaluated as a function of the pre-pulse duration FWHM and is illustrated by black curve in Fig. 2; solid dots infers the simulation data points. The inhomogeneity parameter b decreases with increasing pre-pulse FWHM and take values of the order of ~10^{27} cm^{-4}; the analytical results (blue curve) are in reasonable agreement with the hydrodynamic simulation

Optics EXPRESS

results for $\tau_p \geq 3$ ps. The difference in the two estimates for $\tau_p < 3$ ps may be a consequence of dominance of the electron dynamics in short time scale. The x axis in Fig. 2 is the FWHM of the pedestal/pre-pulse and the figure also implicitly infers the dependence of inhomogeneity parameter on the pre-pulse fluence ($\sim I_{po}\tau_p$). This scaling for b has been used to evaluate the characteristic features of the reflected pulse on the basis of analytical expressions derived in Section 2.

4. Analytical model reflectivity results

4.1 Comparison with experimental results

In order to substantiate the analytical model, it is worthwhile to compare the output from the expressions with experimental observations [23]. The reflectivity of short sub-picosecond pulses from bulk quartz (silica) as a function of fluence has been investigated and in particular the 60 J/cm^2 – 60 fs pulse has been found to show 65% peak (~60% cumulative) reflectivity. The steepness b for the experimental case has to be estimated in order to perform a comparison. The target ionization and expansion begins from the threshold intensity (~10^{11} Wcm^{-2} [22,23]) – about 2 ps before the main pulse. Assuming that ~40% of the laser energy (the fraction in reference case) is absorbed in few skin depths (~$4.5c/\omega_p$), refers that the mean electron temperature T_e ~60 eV. This is consistent with the figure 10 in the referred work [23] and corresponds to a mean electron thermal speed of 3.25×10^8 cms^{-1}. This means that the pre-plasma may extend up to ~6.5 μm and infers inhomogeneity parameter $b\sim 6.5\times10^{26}$ cm^{-4}. This scaling (b) is also consistent with figure 9 of the experimental work [23] where the plasma density decays from the maximum ($\sim 3.3\times10^{23}$ cm^{-3}) to a finite saturation value $\sim 10^{20}$ cm^{-3} in few microns above the target surface (extrapolated up to ~5 μm). Using the square root intensity dependence of the electron temperature, the steepness can be written as $b \propto W^{1/2} \sim I^{1/2}$ and the fluence range depicted in experiment $W \in$ (1-100) Jcm^{-2} consistently gives $b \in$ (0.84-8.39) × 10^{26} cm^{-4}.

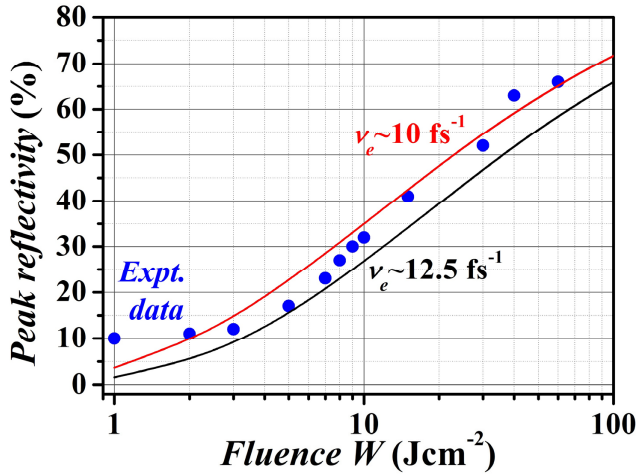

Fig. 3. Comparison of analytical results with experiment [23]: Peak reflectivity as a function of fluence for ν~10 fs^{-1} and ~12.5 fs^{-1}; blue dots refers to measurements.

Figure 3 shows that the analytical results for the peak reflectivity of the pulse (~60 fs) as a function of incident fluence. The red and black curves refer to $\nu \approx 10$ fs^{-1} [23, 42] and Spitzer resistivity [43] $\nu \approx 12.5$ fs^{-1} respectively while the experimental data [23] has been depicted by blue dots in graph. The analytical estimates are in reasonably good agreement with the

experimental observation. Next, these analytical expressions are used to evaluate the features of reflected pulses from PMs.

4.2 Reflection of short pulses*:* parametric analysis

It is evident from the analytical expressions Eqs. (7) and (8) that the reflectivity of the pulses from an inhomogeneous pre-plasma depends primarily on plasma steepness (*b*), pulse width (τ) and damping (i.e. collision frequency ν). For a numerical appreciation of the analytical model, following data set is used for the parametric analysis: $\lambda_o = 0.8$ μm, $\tau_0 = 5$ fs (pulse FWHM), $\tau = 0.6\tau_0$, $\theta = \pi/4$ and $\nu = 10$ fs^{-1}; the pulse parameters taken herein (λ_o, τ_o, τ) are also consistent with the primary laser anticipated to be installed at ELI-ALPS infrastructure [30]. The analytical expressions based on Taylor series expansion is practically applicable for the pulses $\delta\omega/\omega_o = \Delta\omega/2\omega_o \sim 0.1$. For a 5 fs pulse, this ratio is $\delta\omega/\omega_o \sim 0.115$ and hence these analytical expressions are reasonably applicable in the present case, considered herein. In calculations, the effect of an individual parameter on the pulse reflectivity is evaluated by varying it whilst keeping other parameters constant.

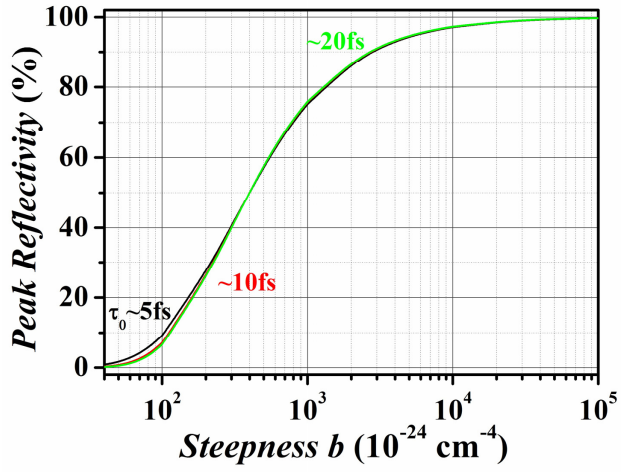

Fig. 4. The peak reflectivity of the pulse as function of density steepness (*b*) for different values of τ_0 and correspond to the standard set of parameters stated in text.

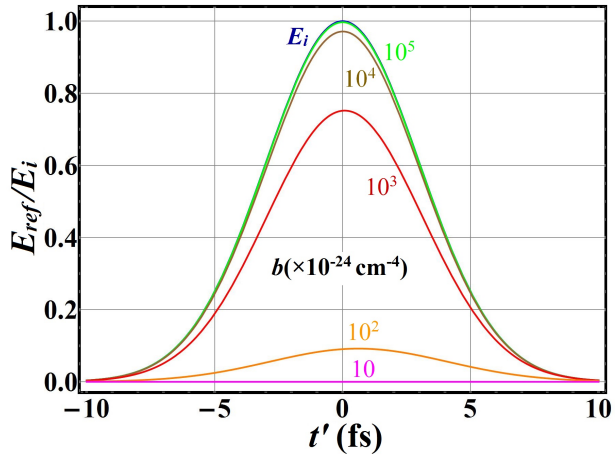

Fig. 5. Electric field profile of the reflected pulse for different values of *b*; the figure corresponds to ν~10 fs^{-1} and standard set of parameters stated in text.

Optics EXPRESS

Figure 4 shows the dependence of the post-reflection peak reflectivity of the pulses on the density steepness b. The peak reflectivity is observed to increases with increasing b and complete reflectance (~99%) is anticipated for $b\sim 3\times10^{28}$ cm^{-4}; this feature is also evident from the corresponding temporal profile of the reflected pulse, shown in Fig. 5 where the pulse is reflected without any significant shape distortion for large values of the steepness. The pulse width of the incident short pulses marginally affects the peak reflectivity, as shown in the Fig. 4.

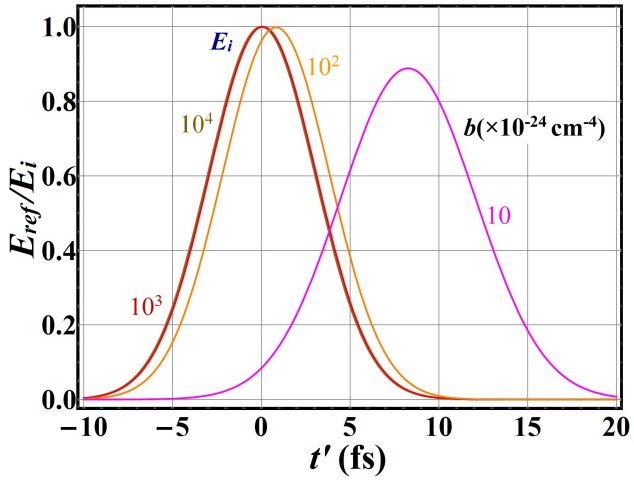

Fig. 6. Electric field profile of the reflected pulse for different values of b; the figure corresponds to collisionless case (ν~0) and standard parameters stated in text.

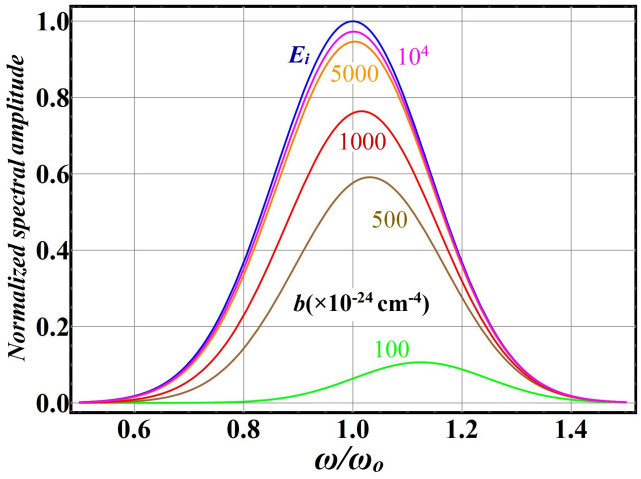

Fig. 7. Pulse spectrum of reflected pulse (corresponding to Fig. 5) for different values of b and figure correspond to the standard set of parameters stated in text.

The post-reflection temporal profile of the short pulses corresponding to collisionless case ($\nu = 0$) for different values of the density steepness b have been shown in Fig. 6; the pulse exhibits nearly instant reflection and is noticed to retain its shape after reflection for large b values. The collisionless case (Fig. 6) in fact refers $\chi << 1$ where the pulse is reflected without significant perturbation in its shape and field intensity. The figure also indicates the decrease in the peak intensity of the reflected pulse for small b values. This nature can be attributed to pulse stretching after the reflection from inhomogeneous plasma; this feature is associated

Optics EXPRESS

with parameter χ as described in the discussion of Section-2. This figure also implicitly demonstrates that the instant reflectivity of the pulse might decay in a realistic situation where plasma expansion coexists with the main pulse interaction, resulting in continuous decrease in b. This effect may give rise to an asymmetric profile of the reflected pulse. However, this deformation is reasonably small for the pulses shorter than the pre-pulse, as b slightly changes during main pulse interaction. For the 5 fs pulses, the plasma instantly expands by 21 nm (for 100 eV electrons) and b (~10^{27} cm^{-4}) slightly changes as 0.96 × 10^{27} cm^{-4}. The frequency spectrum of the reflected pulse is shown in Fig. 7 and the spectral span is nearly same to that of incident pulse. This may be a consequence of limitation of the analysis in the linear regime. Nonetheless, the peak amplitude of the field spectrum decreases for small b and can be understood in terms of larger penetration of the pulse within pre-plasma, resulting in larger attenuation of its amplitude due to finite damping.

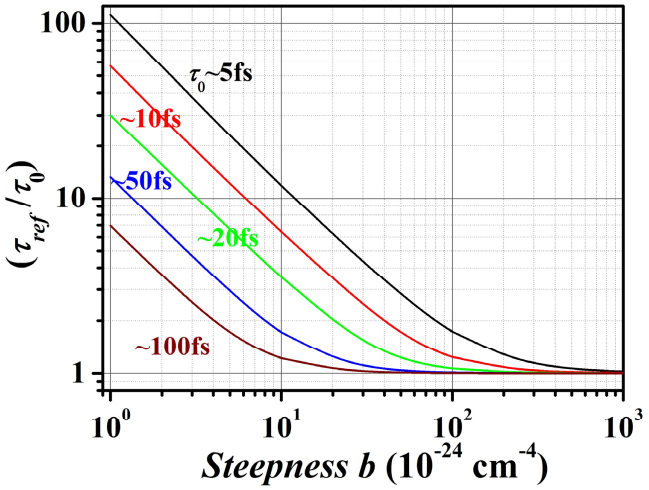

Fig. 8. The temporal width (FWHM) of the reflected pulse (τ_{ref}/τ_0) as function of b for different values of τ_0; figure correspond to the standard parameters stated in text.

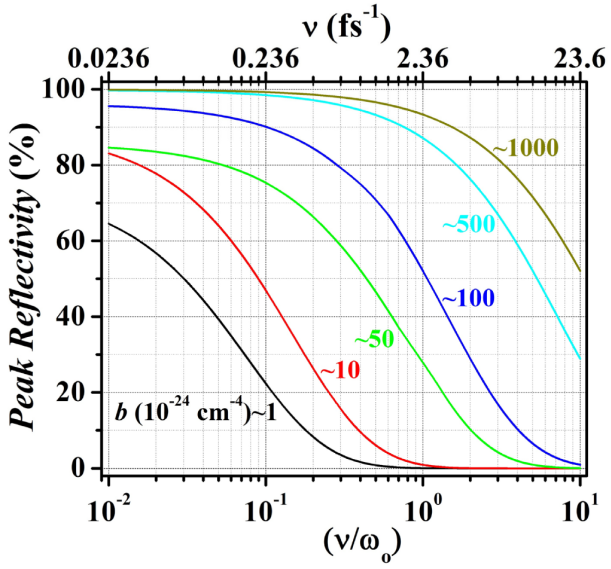

Fig. 9. The peak reflectivity of the pulse as function of collision frequency (ν/ω_o) for different values of the density steepness (b).

Optics EXPRESS

The FWHM of the reflected pulse (τ_{ref}) has been illustrated as a function of b for different values of τ_0 in Fig. 8. The FWHM of the reflected pulse (τ_{ref} / τ_0) decreases with increasing steepness and approaches the incident pulse FWHM (τ_0) for the large values of $b \sim 10^{28}$ cm^{-4}, with significant peak reflectivity (~95%, Fig. 4). Further, the ratio τ_{ref} / τ_0 is seen to take smaller values with increasing the incident pulse width (τ_0) as a consequence of decrease in χ. Figure 9 shows the effect of damping (collision frequency) on the peak reflectivity of the pulse for different values of the inhomogeneity parameter b. The reflectivity is seen to decay with increasing collision frequency and in the collisionless case ($\nu \sim 0$), there is virtually complete reflection (>96%) and weakly depends on the inhomogeneity parameter in the region $b \geq 10^{26}$ cm^{-4}.

It should be mentioned that, analytical results, despite being based on expressions with simplified assumptions, gives a physics insight of the short pulse reflection from the PM set-up. It may also be pointed out that sharp reflection of the shorter pulses without significant distortion could be obtained from PMs with large density steepness. 1D PIC simulations will now be performed in order to validate these analytical predictions.

5. PIC simulation results

The reflection of short pulses from the high (solid) density inhomogeneous plasma has been examined using 1D PIC code [33] to calibrate the analytical model. In this simulation scheme, a 800 nm short duration (τ_0~5 fs, pulse FWHM) s-polarized laser pulse obliquely ($\theta = \pi/4$) interacts with a plasma slab having linear ramp density profile, in the collisionless regime.

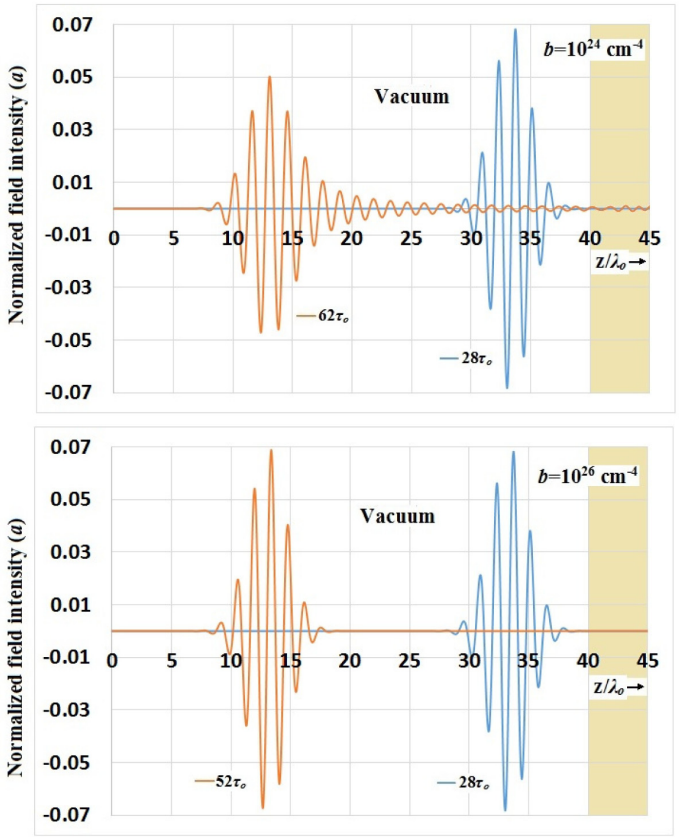

Fig. 10. Simulation results: Snapshot of the normalized electric filed profile of the incident (blue) and reflected (orange) pulse for three different values of the density steepness b = 10^{24} & 10^{26} cm^{-4}; the simulation refers to incident pulse a_o ~0.07 (~10^{16} W/cm^2), τ_{raise} ~4τ and λ_o ~800nm.

Optics EXPRESS

The pulse is simulated using Gaussian temporal profile (in code: Shape 4). The pulse envelop is terminated at a reasonable width so that the amplitude becomes physically insignificant – in code, pulse envelop refers to $\tau_{raise} = 4\tau \approx 2.4\tau_0$. The pulse is physically reflected from plasma layers corresponding to the critical plasma density (n_c). For the short pulse considered herein, it is reasonable to consider the maximum plasma density ($n_{max} \sim 10n_c$) for the simulation. The simulation box is constructed so that the region $0 \le z \le 40\lambda_o$ refers to the vacuum region while the plasma begins with the linear ramp density profile extended up to $40\lambda_o \le z \le 40\lambda_o + (n_{max}/b)$. For the simulation run, the following data has been imbedded as input parameters in the pic code: Pulse amplitude (normalized intensity) $a_o \approx 0.07$ (refers to $\sim 10^{16}$ Wcm^{-2}), cells per wavelength = 100, particles per cells (electron) = 50, initial electron temperature = 100 eV, pulse save steps = $0.05\tau_0$ and cold ions of mass number 60 amu (equivalent to silica) with ~20 particles per cells. In order to optimize the numerical perturbations and ensure a complete pulse after reflection, the snapshots of the reflected pulse are gathered after a long simulation run ($\sim 100\tau_o$) and data has been extracted after each τ_o. The simulation has been performed for two different values of the plasma density ramp steepness (b) 10^{24} and 10^{26} cm^{-4}; the pulse parameters are kept consistent for the calculations as stated in Section 4.2. The snapshots of the propagating pulse in simulation at two different time steps $28\tau_o$ (incident, blue curves) and around $\sim 55\tau_o$ (reflected, orange) are shown in Fig. 10. The snapshot corresponding to $b \sim 10^{26}$ cm^{-4} (in bottom) illustrates nearly complete reflection (98%) and the peak reflectivity is seen to decrease for smaller b values; specifically the pulse displays 71% peak reflectivity in case of $b \sim 10^{24}$ cm^{-4} respectively.

These snapshots have a reasonable agreement with the linear analysis results (Figs. 6 and 9) for collisionless case where the peak reflectivity decreases with decrease in the density steepness. The pulse profile for the case $b \approx 10^{26}$ cm^{-4} is consistent with the respective analytical illustration in Fig. 6 where the profile shape is retained with nearly complete reflection. The magnitude of the peak reflectivity, in the case of lower b (*i.e.* 10^{24} cm^{-4}) is also consistent with the Fig. 9 for the respective case for weak collisions ($\nu \approx 0.01\omega_o$) where it approaches ~70%. It should be noted that the analytical model is based on linear analysis where the instant coupling between incident and reflected pulse, plasma expansion during main pulse interaction, and the nonlinear effects originated from laser intensity and collective plasma influence are ignored. The PIC simulation takes account of these transient effects and is performed for the collisionless case. In contrast to the analytical prediction of symmetrical post-reflection pulses (Figs. 5 and 6), the simulations predict a distortion of reflected pulse shape with decreasing b and slightly extended in space (particularly in rear part). The amplitude distortion of the pulse for smaller b may be attributed to its larger penetration in plasma for weaker inhomogeneity while the pulse extension in rear part may be a consequence of field coupling and nonlinear plasma perturbations.

6. Conclusions

An analysis describing the reflection of broad spectrum ultrashort pulses from an inhomogeneous plasma layers characterized by high density steepness has been performed. The expressions for characteristic temporal/spectral features of the reflected pulse have been derived and their pertinence has been verified with recent experimental results [23]. The pulse reflectivity is shown to be an increasing function of plasma density steepness (inhomogeneity parameter) and marginally influenced by incident pulse duration (FWHM). The broadening of the pulse has also been predicted after reflection and is specified to be a decreasing function of incident pulse width. The pulse reflectivity is drastically influenced by inherent damping (collisions). The analytical estimates for the pulse reflection are found in a reasonable agreement with 1D PIC simulation results for small intensity laser pulses. As an illustrative example, a 5 fs pulse is shown to have 98% peak reflectivity and retains its initial shape after

Optics EXPRESS

reflection without significant distortion for large steepness ($b \geq 10^{26}$ cm^{-4}). Higher contrast pulses could be achieved via appropriate tuning of plasma (PM substrate) and pulse features. The analytical formulation presented herein is quite simplified as it relies on linear calculations of the pulse reflectivity where the plasma mirror configuration (pre-plasma) and reflection are treated subsequently as independent steps. In a realistic scenario, the coexisting optical shuttering (PM formation) and pulse reflection along with other nonlinear effects may certainly limit the applicability of analytical expressions presented herein. It should also be mentioned that the density steepness (b) is a crucial parameter in our analysis and more precise values is needed for accurate prediction of the pulse reflectivity, in particular for the shorter pulses where the pre-plasma generation/expansion exhibits transient behaviour and the electron-ion dynamics may couple in complex manner yielding spatial extension. Another concern is the suitable plasma targets for high repetition rate laser which requires consequent replacement after each shot and promising schemes like optical target positioning device [27,28] or using liquid crystals as target material [44] which allow plasma mirror operation at high repletion rate are proposed. Nevertheless, the analytical formulation illustrated herein, provides a physics notion about characteristic features of the pulse reflected from PMs and the analytical expressions can be utilized in parametric designing of PM in the experimental campaigns. The understanding developed in this study may be of practical significance in establishing the preliminary features of high contrast PM scheme at ELI-ALPS facility.

Funding

ELI-ALPS (Grant agreement GINOP 2.3.6-15-2015-00001); European Cluster of Advanced Laser Light Sources (EUCALL) - European Union's Horizon 2020 research and innovation programme (Grant agreement No. 654220).

Acknowledgements

SKM would like to thank Dr. Daniel Papp for providing Hydro code and its initial briefing. The authors would also like to acknowledge Dr. Andrew Cheesman for his helpful discussions in improving the manuscript text.